Compressive properties of electron beam melted lattice structures with density gradient

Choy, Sing Ying; Wang, Pan; Sun, Chen Nan; Feih, Stephanie; Sin, Wai Jack; Leong, Kah Fai; Wei, Jun

2018

Choy, S. Y., Sun, C. N., Feih, S., Wang, P., Sin, W. J., Leong, K. F., & Wei, J. (2018). Compressive properties of electron beam melted lattice structures with density gradient. Proceedings of the 3rd International Conference on Progress in Additive Manufacturing (Pro-AM 2018), 226-231. doi:10.25341/D4X306

https://hdl.handle.net/10356/88302

https://doi.org/10.25341/D4X306

COMPRESSIVE PROPERTIES OF ELECTRON BEAM MELTED LATTICE STRUCTURES WITH DENSITY GRADIENT

S.Y. CHOY[1,2], C.N. SUN[1,3], S. FEIH[3], P. WANG[3], W.J. SIN[3], K.F. LEONG[1,2], J. WEI[1,3]

[1]*SIMTech-NTU Joint Laboratory, 3D Additive Manufacturing, Nanyang Technological University, 50 Nanyang Avenue, Singapore 639798*

[2]*Singapore Centre for 3D Printing, School of Mechanical & Aerospace Engineering, Nayang Technological University, 50 Nayang Avenue, Singapore 639798*

[3]*Singapore Institute of Manufacturing Technology, 73 Nanyang Drive, Singapore 637662*

ABSTRACT: Lattice structures are used in many applications such as lightweight design, energy absorbers and medical implants. Incorporating a density gradient in the design of lattice structures provides distinctive properties compared to designs with uniform density. In this study, density graded lattice structures of four different architectures were fabricated by electron beam melting technique with Ti-6Al-4V as building material. The samples were tested for compressive properties in comparison to their counterparts with uniform density. Under quasi-static uniaxial loading conditions, density graded samples exhibited more predictable deformation behavior and higher energy absorption than samples with uniform density. Observation with scanning electron microscopy showed that the fracture surfaces of the compressed density graded samples changed across the structure according to strut diameter. Finite element simulation was also conducted to compare the structural stiffness and to identify locations of highest stresses of the different lattice designs during deformation, and the results were compared with the deformation behavior observed from experiments. The distinctive properties of density graded lattice designs demonstrated in this study encourage further research to achieve advanced and tailored functionality.

KEYWORDS: 3D printing, additive manufacturing, electron beam melting, lattice structure, compression

INTRODUCTION

Lattice structures are porous structures consisting of regular repeating unit cells. Lattice design approaches are used in many applications including lightweight structures, energy absorbers, medical implants, and heat exchangers. The properties of these structures can be varied by manipulating the material, unit cell shape, and relative density of the structure. Conventional manufacturing processes have limited design freedom, and can only produce relatively simple geometries of lattice structures which lack the advanced functionality to meet the requirements of many applications. On the other hand, additive manufacturing (AM) techniques provide flexibility in structural design and become an outstanding technique to fabricate lattice structure with various internal architecture designs and complex topology with density gradient. Many AM research studies have been conducted by fabricating different design of lattice structure. Majority of the researchers studied lattice designs with uniform density which includes but is not limited to the work done byAhmadi et al. (2015),Hazlehurst et al. (2014), Parthasarathy et al. (2011), and Sudarmadji et al. (2011). Fewer studies focused on lattice structure with density gradient. Studies

Proc. Of the 3rd Intl. Conf. on Progress in Additive Manufacturing (Pro-AM 2018)
Edited by Chee Kai Chua, Wai Yee Yeong, Ming Jen Tan, Erjia Liu and Shu Beng Tor

Published by Nanyang Technological University
ISSN: 2424-8967 :: https://doi.org/10.25341/D4X306

of density graded lattice structures have been undertaken by Grunsven et al. (2014) on diamond design, Li et al. (2016) on rhombic dodecahedron design, Maskery et al. (2016a), and Maskery et al. (2016b) on body-centred-cubic design. But the density gradient in the design of all these research studies was varied in a step-wise manner. In this study, we fabricated lattice structures with density varied continuously and linearly using electron beam melting (EBM) process. Compression tests, fracture surface study and finite element simulation were performed to compare the mechanical properties of samples with density gradient and uniform density.

MATERIALS AND METHODS

Four density graded lattice structures (denoted by FGM) were designed with 3-matics (Materialise NV) as shown in Figure 1. The density was changed by varying the lattice strut diameter linearly and continuously from 0.6 mm to 1.2 mm. The unit cell of the structures had the length of 3mm for every strut in C1 and C2 designs and 2.5mm for every strut in H1 and H2 designs. The sample size (X × Y × Z) were 18mm × 18 mm × 16 mm, 16mm × 18 mm × 18 mm, 18mm × 21 mm × 13 mm, and 18mm × 13 mm × 21 mm for C1, C2, H1 and H2 respectively. The designed porosity was 82% for C1 and C2, 85% for H1 and H2. Another four lattice structures with uniform density (denoted by UNIFORM) for comparison with density graded samples had the strut diameter of 0.9 mm. The material volume of the samples with uniform density was the same as for their respective density graded designs and hence the same for their designed porosities. The printing of the lattice structures was performed by an Arcam A2X EBM system (software version 3.2, accelerating voltage 60,000 V, layer thickness 50 μm, Arcam AB standard build theme for Ti-6Al-4V alloy). Pre-alloyed Ti-6Al-4V (supplied by Arcam AB, grade 5) powder with spherical particle size was used in this study. After cleaning the semi-sintered surrounding powder by a powder recovery system (PRS), the support structures were removed by cutting and slip joint pliers. The detailed preparation and fabrication can be found in our previous reports (Wang et al. (2015), Wang et al. (2017)).

The density of the lattice strut was determined by Archimedes' principle. The mass of the sample in air and in ethanol was measured by weighing device (Mettler Toledo XS204). The density of the lattice structure was calculated by dividing the sample mass with sample volume. The sample volume was determined by multiplying the length, width and height of the sample which were measured with a caliper. The relative density was calculated by dividing the sample density with a theoretical density of bulk Ti-6Al-4V (4.43 g/cm^3). The porosity was determined from the percentage of void volume in the sample. The void volume was the ratio of the difference between material volume and sample volume to the sample volume. The material volume was back-calculated from the division of sample mass with strut density. The compression test was performed by a universal mechanical testing machine (Shimadzu Autograph AG-X Plus) with 0.06 per minute strain rate. Photographs were taken during the compression process. The energy absorption per unit volume was determined from the area under the stress-strain curve up to the densification strain before the curve rises steeply. Fracture surfaces of the compressed samples were observed with scanning electron microscope (SEM) (JEOL JSM-5600LV). The finite element study was performed with Abaqus software (version 2016). The input values for the material properties in the simulation were 4.42 g/cm^3, 114.5 GPa and 0.342 for density, Young Modulus and Poison's ratio, respectively. The geometry of the simulated samples was generated by FLatt Pack software (Added Scientific Ltd.) with hexahedral shaped elements. A linear

perturbation analysis was used to study the stress distribution within a sample during the initial compression step at 5% strain.

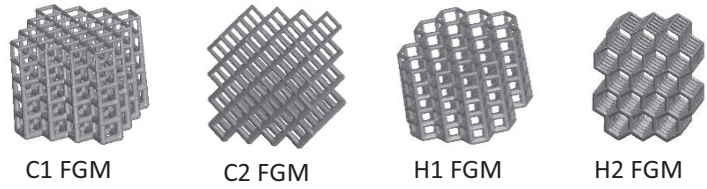

Figure 1. Four designs of density graded lattice structures studied in this work.

RESULTS AND DISCUSSION

The density of the lattice struts for all samples were in the range of 99.51% to 99.95%. These densities were near to full density and the printing process parameters were deemed to be favorable. The measured porosity and relative density were tabulated in Table 1. Comparing to the designed porosities of 82% for C1, C2, and 85% for H1, H2, the deviation of measured porosity from the designed value for all the samples was in the range of 0.09% to 2.11%.

Table 1. Porosity and relative density of lattice structures.

Sample	Porosity (%)		Relative density (%)	
	FGM	UNIFORM	FGM	UNIFORM
C1	81 ± 0.08	82 ± 0.10	19 ± 0.09	18 ± 0.11
C2	82 ± 0.09	82 ± 0.11	18 ± 0.09	18 ± 0.10
H1	83 ± 0.11	84 ± 0.05	17 ± 0.10	16 ± 0.05
H2	83 ± 0.02	85 ± 0.20	17 ± 0.03	15 ± 0.19

The deformation behavior of all the density graded samples during quasi-static axial loading condition occurred in a progressive collapse manner as illustrated in Figure 2. The difference in unit cell shape among the four different lattice designs did not affect the deformation behavior. The same lattice designs with uniform density which had the same material volume as the density graded samples deformed differently according to unit cell shape. As shown in Figure 3, the uniform density samples of C1 and H1 designs collapsed layer by layer in a stochastic manner assumingly determined by minor manufacturing defects, while the uniform density samples of C2 and H2 designs failed with a diagonal shear band across the whole structure from corner to corner. The progressive collapse pattern of the density graded structures was more predictable and might be useful in applications which require protection at the denser side of the structure during compression. The specific energy absorption of all four different lattice designs was higher in density graded samples compared to their respective uniform density samples as shown in Figure 4. This may be attributed to the contribution of density values which had power factor of more than one in the energy absorption equation for a cellular structure with uniform density created by Gibson and Ashby (1997) as shown in equation (1) below. The absorbed energy increased by power factor in a density graded sample when the structure deformed progressively.

$$\frac{W}{E_s} = 0.3\frac{\sigma_{ys}}{E_s}\left[\frac{\rho}{\rho_s}\right]^{1.5}[\epsilon - \epsilon_0] \quad (1)$$

where W is energy absorption, E_s is Young's modulus of solid material, σ_{ys} is yield stress, ρ/ρ_s is relative density of cellular solid, ϵ is strain, ϵ_0 is strain at the end of the linear elastic regime.

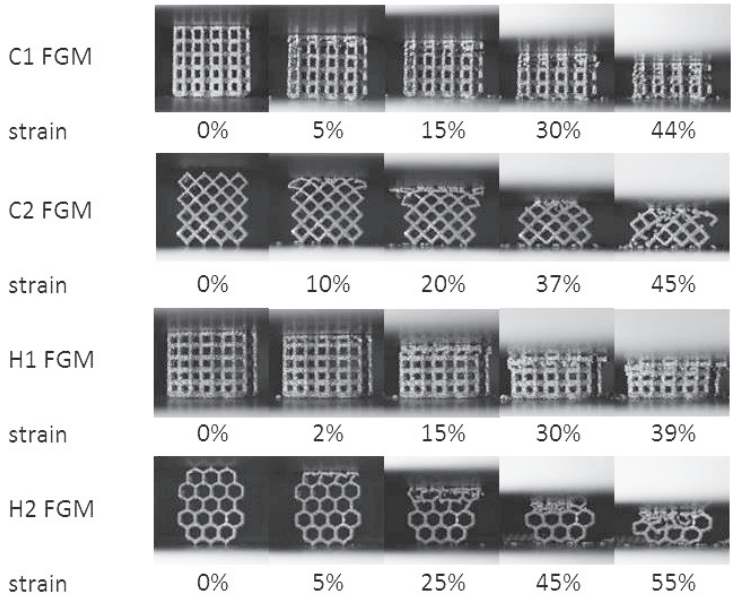

Figure 2. Progressive collapse pattern exhibited by density graded lattice structures.

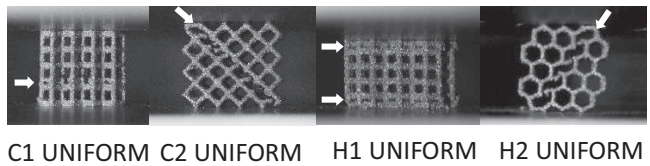

Figure 3. Random layer collapse and diagonal shear band failure exhibited by lattice structures with uniform density.

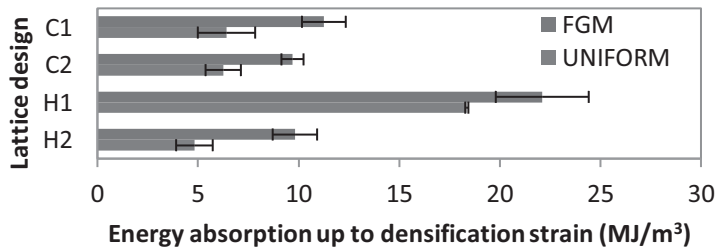

Figure 4. Energy absorption up to densification strain for lattice structures.

The fracture surfaces of the compressed samples were observed under SEM. All density graded samples had coarser fracture surfaces with deeper ductile dimples at the top of the structure where the struts were thinnest compared to the fracture surfaces of the struts at the bottom of the structure as illustrated in Figure 5 indicating different contributions of tensile and shear loading influencing stress triaxiality. On the other hand, the fracture surfaces at the top and bottom struts of all the uniform density samples were similar which were coarse with ductile dimples. These results suggest a variation in fracture surface property of a density graded lattice structure. A previous study on similar lattice designs printed by selective laser melting technique also showed similar results in fracture surfaces, deformation behavior and energy absorption (Choy et al. (2017).

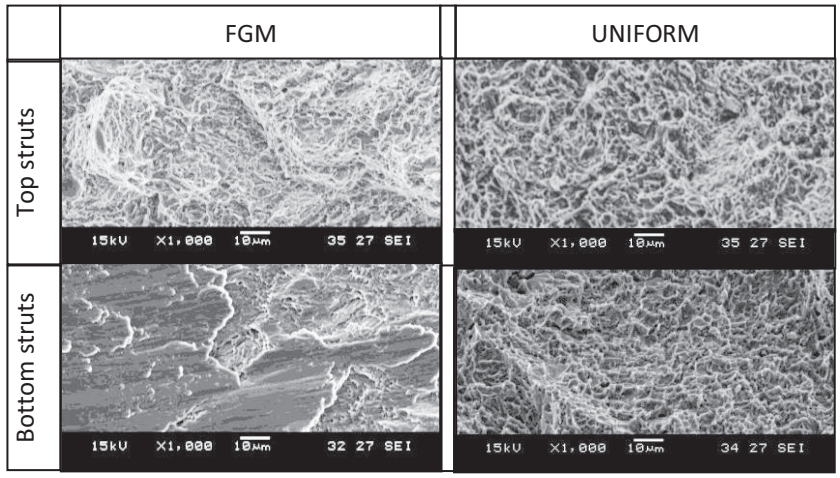

Figure 5. Comparison of fracture surfaces at the top struts and bottom struts of the structures between density graded and uniform density for C2 design.

Finite element simulation results are shown for the C2 lattice design, and the Mises stress contours at 5% strain during compression are shown in Figure 6. The simulation results agreed with the experimental results as the high stress areas were concentrated at the thinner top struts of the structure where failure started for density graded sample, while the uniform density sample exhibited uniform stress distribution.

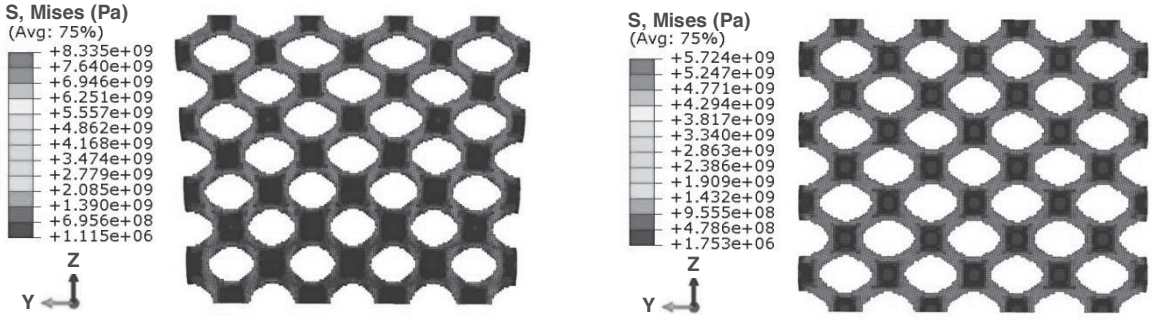

C2 FGM C2 UNIFORM

Figure 6. Comparison of Mises stress contours for C2 design at 5% strain.

CONCLUSIONS

As demonstrated with the four different lattice designs fabricated by EBM technique in this study, incorporating density gradients in lattice designs resulted in distinctive deformation behavior which was more predictable and superior energy absorption compared to the uniform density design. There was variation in the fracture surface patterns within the density graded structures according to the diameter of lattice struts. Structural stiffness and locations of highest stresses at the initial step of the compression had been identified with the finite element study.

ACKNOWLEDGMENTS

We wish to acknowledge the financial support of SIMTech-NTU Joint Laboratory (3D Additive Manufacturing) and A*STAR Industrial Additive Manufacturing Program: Work Package 3 (Electron Beam Melting) [Grant No. 132 550 4103].

REFERENCES

Ahmadi, Seyed Mohammad, Saber Amin Yavari, Ruebn Wauthle, Behdad Pouran, Jan Schrooten, Harrie Weinan and Amir A. Zadpoor. (2015), "Additively manufactured open-cell porous biomaterials made from six different space-filling unit cells: The mechanical and morphological properties." *Materials,* 8, 1871-1896.

Choy, S. Y., C. N. Sun, K. F. Leong and J. Wei. (2017), "Compressive properties of functionally graded lattice structures manufactured by selective laser melting." *Materials & Design,* 131, 112-120.

Gibson, Lorna J. and Michael F. Ashby. *Cellular solids: Structure and properties*. 2nd edition ed. Cambridge ; New York: Cambridge University Press, 1997.

Grunsven, William van, Everth Hernandez-Nava, Gwendolen C. Reilly and Russell Goodall. (2014), "Fabrication and mechanical characterisation of titanium lattices with graded porosity." *Metals,* 4, 401-409.

Hazlehurst, K. B., C. J. Wang and M. Stanford. (2014), "An investigation into the flexural characteristics of functionally graded cobalt chrome femoral stems manufactured using selective laser melting." *Materials and Design,* 60, 177–183.

Li, Shujun, Shuo Zhao, Wentao Hou, Chunyu Teng, Yulin Hao, Yi Li, Rui Yang and R. D. K. Misra. (2016), "Functionally graded ti-6al-4v meshes with high strength and energy absorption." *Advanced Engineering Materials,* 18 (1), 34-38.

Maskery, I., N.T. Aboulkhair, A .O. Aremu, C.J. Tuck, I.A . Ashcroft, R.D. Wildman and R.J.M. Hague. (2016b), "A mechanical property evaluation of graded density al-si10-mg lattice structures manufactured by selective laser melting." *Materials Science & Engineering A,* 670, 264-274.

Maskery, Ian, Alexandra Hussey, Ajit Panesar, Adedeji Aremu, Christopher Tuck, Ian Ashcroft and Richard Hague. (2016a), "An investigation into reinforced and functionally graded lattice structures." *Journal of Cellular Plastics*, 1-15.

Parthasarathy, J., B. Starly and S. Raman. (2011), "A design for the additive manufacture of functionally graded porous structures with tailored mechanical properties for biomedical applications." *Journal of Manufacturing Processes,* 13, 160-170.

Sudarmadji, N., J. Y. Tan, K. F. Leong, C. K. Chua and Y. T. Loh. (2011), "Investigation of the mechanical properties and porosity relationships in selective laser-sintered polyhedral for functionally graded scaffolds." *Acta Biomaterialia,* 7, 530-537.

Wang, P., M.L.S. Nai, W.J. Sin and J. Wei. (2015), "Effect of building height on microstructure and mechanical properties of big-sized ti-6al-4v plate fabricated by electron beam melting." *MATEC Web of Conferences,* 30, 02001.

Wang, P., W.J. Sin, M.L.S. Nai and J. Wei. (2017), "Effects of processing parameters on surface roughness of additive manufactured ti-6al-4v via electron beam melting." *Materials,* 10 (1121).